Gradient-Boosting Classifiers Combining Vessel Density and Tissue Thickness Measurements for Classifying Early to Moderate Glaucoma

CHRISTOPHER BOWD, AKRAM BELGHITH, JAMES A. PROUDFOOT, LINDA M. ZANGWILL, MARK CHRISTOPHER, MICHAEL H. GOLDBAUM, HUIYUAN HOU, RAFAELLA C. PENTEADO, SASAN MOGHIMI, AND ROBERT N. WEINREB

• PURPOSE: To compare gradient-boosting classifier (GBC) analysis of optical coherence tomography angiography (OCTA)-measured vessel density (VD) and OCT-measured tissue thickness to standard OCTA VD and OCT thickness parameters for classifying healthy eyes and eyes with early to moderate glaucoma.

• DESIGN: Comparison of diagnostic tools.

• METHODS: A total of 180 healthy eyes and 193 glaucomatous eyes with OCTA and OCT imaging of the macula and optic nerve head (ONH) were studied. Four GBCs were evaluated that combined 1) all macula VD and thickness measurements (Macula GBC), 2) all ONH VD and thickness measurements (ONH GBC), 3) all VD measurements from the macula and ONH (vessel density GBC), and 4) all thickness measurements from the macula and ONH (thickness GBC). ROC curve (AUROC) analyses compared the diagnostic accuracy of GBCs to that of standard instrument-provided parameters. A fifth GBC that combined all parameters (full GBC) also was investigated.

• RESULTS: GBCs had better diagnostic accuracy than standard OCTA and OCT parameters with AUROCs ranging from 0.90 to 0.93 and 0.64 to 0.91, respectively. The full GBC (AUROC = 0.93) performed significantly better than the ONH GBC (AUROC = 0.91; $P = .036$) and the vessel density GBC (AUROC = 0.90; $P = .010$). All other GBCs performed similarly. The mean relative influence of each parameter included in the full GBC identified a combination of macular thickness and ONH VD measurements as the greatest contributors.

• CONCLUSIONS: GBCs that combine OCTA and OCT macula and ONH measurements can improve diagnostic accuracy for glaucoma detection compared to most but not all instrument provided parameters. (Am J Ophthalmol 2020;217:131–139. © 2020 Elsevier Inc. All rights reserved.)

OPTICAL COHERENCE TOMOGRAPHY ANGIOGraphy (OCTA) is a relatively new optical imaging technology that allows noninvasive measurement of vessel density using 2 subsequent aligned OCT images to detect between-image changes in relative voxel position that indicate the presence of flowing blood. OCTA vessel density measurements (percentage of OCTA image occupied by regions of flowing blood) have been shown to be lower in glaucoma suspect and glaucoma eyes than in healthy eyes, to decrease with increasing glaucoma severity as described by decreasing standard automated perimetry visual field (VF) mean deviation (MD) and to be lower in the corresponding perimetrically unaffected hemiretina of eyes with hemifield-specific VF defects.[1–10] In addition, baseline parapapillary and macular vessel density measurements are reportedly predictive of more rapid glaucoma-related thinning of the retinal nerve fiber layer (RNFL),[11] and a significant decrease in superficial macular vessel density has been reported over time in glaucoma eyes in conjunction with a thinning of the ganglion cell complex (GCC) (Hou H. and colleagues. IOVS 2019; 59:ARVO E-Abstract 3218).

Current OCTA instruments provide limited analytics beyond global and local vessel density measurements obtained from the perifoveal and peripapillary regions. Available numerical vessel density measurements are difficult to assess in part because comparisons to standard normative measurements from healthy eyes used to determine measurements outside of normal limits are not available. Therefore, vessel density measurements obtained using OCTA currently are difficult to interpret beyond subjective visual inspection of en face images and comparison of relative regional vessel densities.

Studies have shown over the last decades that machine learning (ML) models developed from information available in optic nerve head photographs, optical imaging measurements, and visual field measurements, alone and combined, can improve classification of healthy and glaucoma patient eyes compared to expert assessment, raw measurements, and commercially available instrument-

AJO.com Supplemental Material available at AJO.com.
Accepted for publication Mar 17, 2020.

Viterbi Family Department of Ophthalmology, Hamilton Glaucoma Center and Shiley Eye Institute, University of California San Diego, La Jolla, California, USA.

(Diagnostic Innovations in Glaucoma Study [DIGS] NCT00221897).

Inquiries to: Christopher Bowd, Hamilton Glaucoma Center, Department of Ophthalmology, University of California San Diego, La Jolla, California 92037-0946, USA; e-mail: cbowd@ucsd.edu

0002-9394/$36.00
https://doi.org/10.1016/j.ajo.2020.03.024

provided measurement parameters.[12–34] Results provided by ML models allow relatively easy assessment because they can provide output in the form of probability of disease based on information learned from training data. The current study determined whether ML models trained and tested using OCTA vessel density measurements could improve disease classification compared to vessels density measurements alone. The authors also compared and combined localized OCTA vessel density measurements with localized OCT tissue thickness measurements to determine whether combining available regional measurements would improve classification, to evaluate whether combining macular and optic nerve head measurements could contribute to clinical decision making.

MATERIALS AND METHODS

THIS WAS A CROSS-SECTIONAL COMPARISON OF DIAGnostic tools involving a group of patients with primary open-angle glaucoma, as defined below, and a group of healthy control participants from the DIGS (Diagnostic Innovations in Glaucoma Study) trial. The DIGS trial is an ongoing prospective, longitudinal study conducted at the Hamilton Glaucoma Center, University of California, San Diego, designed to evaluate anatomical structures in glaucoma. Details of the DIGS protocol have been described elsewhere.[34] All methods adhered to the tenets of the Declaration of Helsinki and the Health Insurance Portability and Accountability Act and were approved by the Institutional Review Board of the University of California, San Diego.

• **PARTICIPANTS:** Eligible participants had best corrected visual acuity of 20/40 or better and open angles on gonioscopy at study entry. All participants were 40 years old or older. Participants were excluded if they had a history of intraocular surgery (except for uncomplicated cataract or uncomplicated glaucoma surgery). Eyes with coexisting retinal disease, uveitis, or nonglaucomatous optic neuropathy also were excluded. Diabetic participants with no evidence of retinal involvement were included.

Eyes of healthy participants had healthy appearing optic discs and RNFLs OU based on masked assessment of digital stereoscopic photographs with no history of repeatable, abnormal VF results by Humphrey Visual Field Analyzer II with 24-2 testing using the Swedish interactive thresholding algorithm (Carl Zeiss Meditec, Dublin, California) and no history of elevated intraocular pressure (all intraocular pressure was ≤21 mm Hg) in either eye. Normal VFs were defined as those with MD and pattern standard deviation within 95% confidence interval (CI) and a glaucoma hemifield test result within normal limits.

Glaucoma patient eyes had at least 2 consecutive and reliable VF examinations with either pattern standard deviation of ≥5% or a glaucoma hemifield test result outside of the 99% normal limits with similar patterns of glaucoma-related defects in consecutive examinations. Severity of glaucoma was restricted from early to moderate with MD ≥ −12 dB.

• **VISUAL FIELD TESTING:** All VFs were evaluated by University of California San Diego Visual Field Assessment Center personnel based on a standardized protocol.[35] VFs with fixation losses of more than 33% or false negative errors or more than 15% false positive errors were automatically excluded. VFs exhibiting a learning effect (ie, initial tests with reduced sensitivity followed by consistent improvement in a series of tests) also were excluded. VFs were further reviewed for lid and rim artifacts, fatigue effects, evidence that the visual field results were due to a disease other than glaucoma (eg, homonymous hemianopia), and inattention. Test results indicating such characteristics were excluded.

• **OPTICAL IMAGING:** The commercially available Avanti Angiovue (Optovue Inc. Fremont, California) combines OCTA and OCT imaging in a single system. Avanti Angiovue OCTA (software version 2017.1.0.151) and OCT (software version 5.6.3.0) images of the macula and optic nerve head (ONH) were obtained using the Avanti on the same day by the same instrument operator. The Avanti system for measuring vessel density and tissue thickness has been described previously.[36]

For OCTA vessel density measurements, each volume is composed of 2 consecutive B-scans captured at each fixed position. The instrument-specific split-spectrum amplitude decorrelation angiography method is used to capture the dynamic motion of the red blood cells between consecutive B-scans to provide a high-resolution 3-dimensional visualization of the perfused retinal vasculature.[36] Vessel density is calculated automatically as the proportion of measured area occupied by flowing blood vessels defined as pixels having decorrelation values acquired by the split-spectrum amplitude decorrelation angiography algorithm above the threshold level.

Avanti high-density 6- × 6-mm^2 field of view scans centered on the macula and high density 4.5- × 4.5-mm^2 field of view scans centered on the ONH were acquired and included in the analysis. Macula scan parafoveal measurements were obtained within an annular region with an inner diameter of 1 mm and an outer diameter of 6 mm. To obtain OCTA vessel density measurements, each scan was automatically segmented by the Angiovue software to visualize the instrument-defined macular superficial capillary plexus and deep capillary plexus. The ONH circumpapillary measurements are obtained from within a 10-pixel-wide annulus with an inner diameter of 3.45 mm.

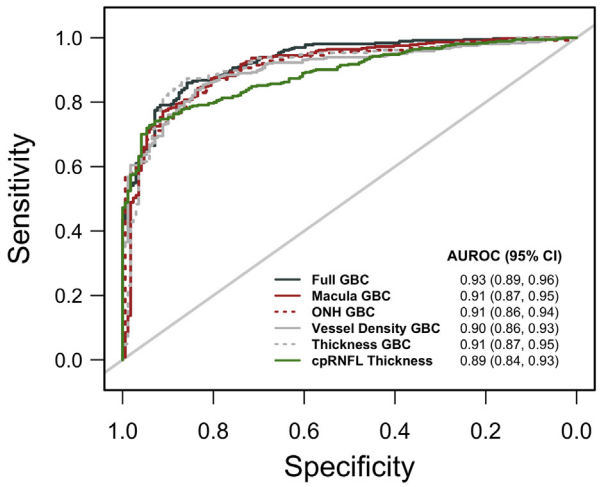

FIGURE 1. Area under the receiver operating characteristic curve (AUROC) plots for each gradient-boosting classifier (GBC).

GCC, composed of RNFL, ganglion cell layer, and inner plexiform layer, thickness and circumpapillary RNFL (cpRNFL) thickness measurements derived from the OCTA scans also were included in the analyses. All measurements were included in standard clinical printouts that can be automatically exported from the Avanti instrument.

To construct parsimonious ML models, 18 macula OCTA parameters were selected from the superficial and deep capillary plexuses; 8 ONH OCTA parameters including parameters with and without large vessels removal; 9 macula OCT GCC thickness parameters; and 3 ONH OCT cpRNFL thickness parameters. Chosen parameters Results are shown in Supplemental Tables 1 and 2.

OCTA and OCT image quality review was completed according to University of California San Diego Imaging Data Evaluation and Analysis reading center standard protocol. Images with a quality index (QI) of <4, poor clarity, residual motion artifacts visible as irregular vessel patterns, or disc boundaries on the enface angiogram, image cropping, or local weak signal due to vitreous opacity, or segmentation errors that could not be corrected were excluded.

• **GRADIENT-BOOSTING CLASSIFIER:** The gradient-boosting classifier (GBC) is an ensemble classifier that attempts to decrease error by resampling and varying the weights for individual weak learners in order to increase classification accuracy.[37] In an empirical comparison study of supervised learning algorithms comparing random forests and boosted decision trees, the GBC had the best overall performance.[38] Motivated by this success, the authors chose to use gradient boosting as the classifier. An advantage of GBC is that it provides output in the form of probability of glaucoma that may be more useful for clinical interpretation than global or local percentage of vessel

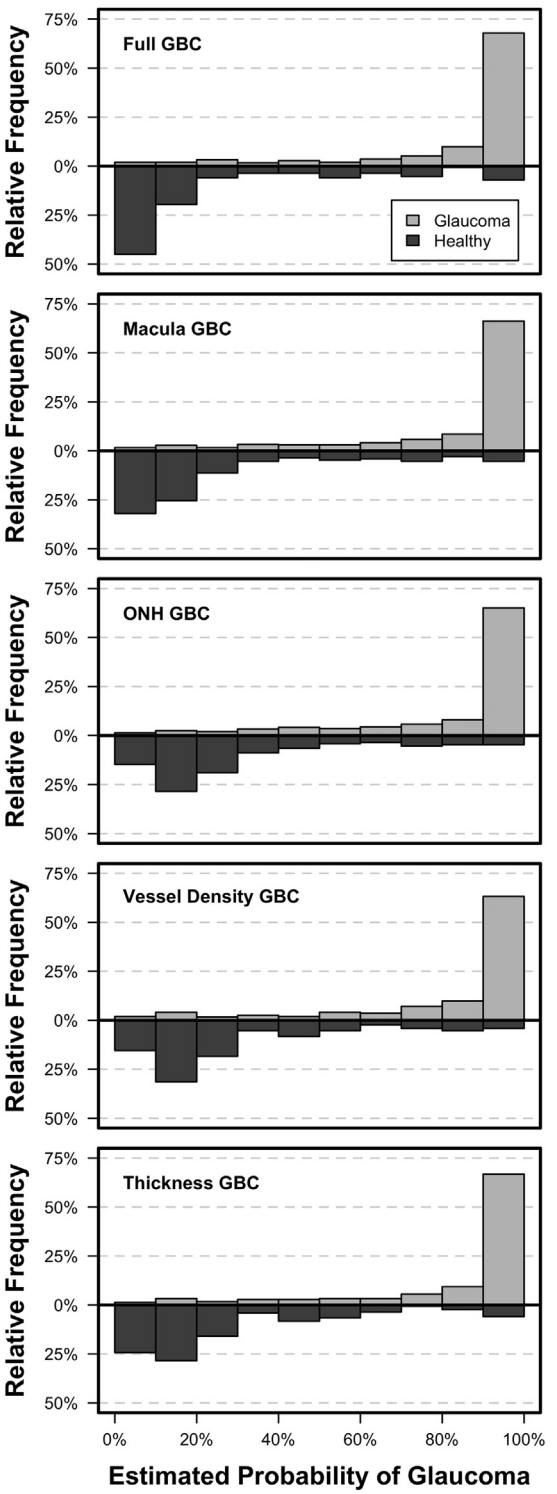

FIGURE 2. Estimated probability of glaucoma from each gradient-boosting classifier (GBC) for healthy and glaucoma images.

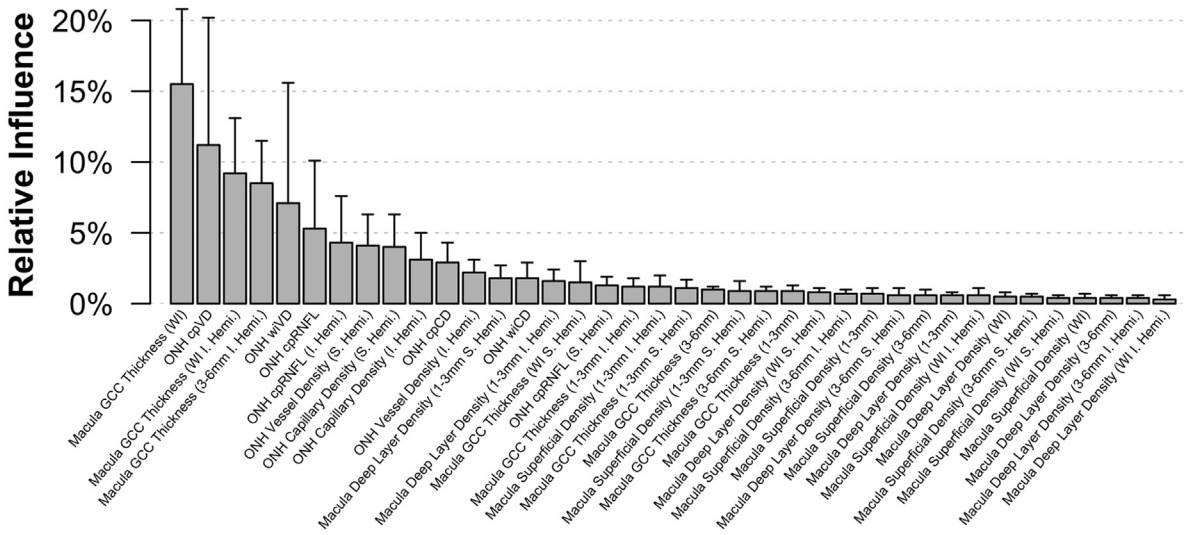

FIGURE 3. Mean relative influence over each cross-validation fold in the full gradient-boosting classifier (Full GBC). The upper bar represents the maximum relative influence observed.

density and tissue thickness measurements alone. GBCs also provide a metric to assess the relative influence of each parameter included in the classifier.[39]

Up to 5 images from each healthy and each patient eye obtained longitudinally were included to increase the sample size and generate more generalizable models, resulting in 169 images of healthy eyes and 364 images of glaucoma eyes. Because multiple images were included from a single studied eye, images were initially weighted by the number of images available for each eye (eg, for an eye providing 5 images, each would be included in the model with an initial weight of 0.2). Separate from the 10-fold cross-validation used to assess model performance (described below), a 5-fold cross-validation was used within each of the 10 training sets to select the optimal number of boosting iterations and prevent overfitting the training data. Means and ranges of the relative influence of each variable included in the full GBC across all cross-validation folds are reported.

• **STATISTICAL ANALYSES:** We developed 4 GBCs combining 1) all macula vessel density and thickness measurements (macula GBC); 2) all ONH vessel density and thickness measurements (ONH GBC); 3) all vessel density measurements from the macula and ONH (vessel density GBC); and 4) all tissue thickness measurements from the macula and ONH (thickness GBC) to compare models based on different location-specific measurements from each other and to compare models based on different structural measurements from each other. A fifth full GBC was also developed combining all Avanti parameters included in the above-described GBCs to determine if combining macula and optic nerve measurements would improve classification overall. An improvement in classification here would suggest that imaging both the macula and the optic nerve could improve diagnostic accuracy in patients with early to moderate glaucoma.

Areas under receiver operating characteristic curves (AUROCs) and sensitivities at fixed specificities of 80%, 85%, 90%, and 95% were used to describe and compare the ability of individual vessel density and tissue thickness parameters and GBCs to distinguish glaucomatous eyes from healthy eyes. Estimates of the probability of glaucoma given by GBCs were calculated by using logistic regression.

A 10-fold cross-validation was used to provide out-of-sample predictions for each logistic and GBC to avoid overly optimistic estimates of classification accuracy. First, the full complement of healthy participants and glaucoma patients (and each of their contributed images) was randomly divided into 10 approximately equal, exhaustive, and mutually exclusive subsets. Next, each model was trained on 9 subsets and subsequently used to generate out-of-sample predictions of the probability of glaucoma on the tenth subset. This sequence was repeated 10 times, with each subset serving as the test set once, so that each tested subject was never part of its training set and was tested only once.

Bias-corrected CI and hypothesis tests for AUCs were conducted using a clustered bootstrap with 2,000 resamples. Due to the exploratory nature of this analysis, no type I error correction for multiple comparisons was applied (as recommended by Bender and Lange[40]). GBC modeling and all statistical analyses were performed using R version 3.5.2 software (R Foundation, Vienna, Austria). The R programming language is an open-source statistical software available free, as is the "gbm" application used for GBC modeling herein.[41,42]

TABLE 1. Patient and Eye Characteristics by Diagnosis

	Diagnosis		
	Healthy (n = 60 Patients; 108 Eyes)	Glaucoma (n = 143 Patients; 193 Eyes)	*P* Value
Age, y	61.5 (58.9-64.1)	72.3 (70.6-73.9)	**<.001**
Females	75.0%	50.3%	**.001**
Race			
Nonwhite	45.0%	35.0%	.073
White	53.3%	65.0%	
Unknown	1.7%	0.0%	
Hypertension	40.0%	55.9%	**.046**
Diabetes	3 (5.0%)	24 (16.8%)	**.024**
MD, dB	0.05 (−1.17 to 1.27)	−5.70 (−6.50 to −4.90)	**<.001**
IOP, mm Hg[a]	15.0 (13.9-16.1)	14.5 (13.8-15.2)	.451
AL, mm[b]	23.9 (23.5-24.2)	24.4 (24.2-24.6)	**.014**
CCT, μm[c]	547.7 (536.5-558.8)	536.8 (529.6-543.9)	.109
Disc or BMO Area, mm^2	1.9 (1.8-2.1)	1.9 (1.8-2.0)	.672

AL = axial length; BMO = Bruch's membrane opening; CCT = central corneal thickness; dB = decibel; IOP = intraocular pressure.

Mean values and 95% confidence intervals are shown for continuous variables. Statistical significance of differences in continuous and categorical variables were determined by 2-sample *t*-tests and Fisher exact tests for patient level variables (respectively) and linear mixed effects models for eye level variables. Missing [a]29, [b]7, and [c]11 values. Bolded *P*-values indicate statistically significant difference with $P \leq .05$.

RESULTS

THE STUDY INCLUDED 108 EYES OF 60 HEALTHY STUDY PARticipants and 193 eyes of 143 glaucoma patients. Summary demographic variables and measurements are shown in Table 1. Glaucoma patients were significantly older than healthy participants (mean = 72.3 years old [95% CI, 70.6-73.9 years] vs 61.5 years [95% CI, 58.9-64.1 years], respectively; $P < .001$) at the time of first examination. In addition, glaucoma patients had a significantly higher rate of systemic hypertension (55.9% vs 40%, respectively; $P = .046$) and diabetes (16.8% vs 5.0%, respectively; $P = .024$) than healthy participants. As expected, glaucoma eyes had a lower VF MD than healthy eyes (−5.70 dB vs. 0.05 dB, respectively; $P < .001$; values presented in Table 1 are MD at the time of first imaging visit if multiple imaging visits were included). Glaucoma patients also had a slightly longer mean axial length (24.4 mm [95% CI, 24.2-24.6 mm] for glaucoma eyes and 23.9 mm [95% CI, 23.5-24.2 mm] for healthy eyes; $P = .014$).

The standard OCTA and OCT parameters with the highest AUROC were whole-image GCC thickness (AUROC = 0.91; 95% CI, 0.86-0.94) and whole-image vessel density (AUROC = 0.91; 95% CI, 0.86-0.94), followed by cpRNFL thickness (AUROC = 0.89; 95% CI, 0.84-0.93) and perifoveal superficial vessel density measured within an annulus between 3 and 6 mm from the fovea (AUROC = 0.84; 95% CI, 0.78-0.89). AUROCs and sensitivities at fixed specificities of 80%, 85%, 90%, and 95% for all investigated OCTA and OCT parameters are shown in Supplemental Table 1.

TABLE 2. Predictive Performance Metrics

		Sensitivity At				
	AUROC (95% CI)	80% Spec.	85% Spec.	90% Spec.	95% Spec.	AUROC *P* Value vs Full GBC
Full GBC	0.93 (0.89-0.96)	87.1%	86.0%	79.1%	64.6%	-
Macula GBC	0.91 (0.87-0.95)	87.6%	80.8%	78.0%	65.7%	.105
ONH GBC	0.91 (0.86-0.94)	86.3%	81.3%	73.9%	66.2%	**.036**
Vessel Density GBC	0.90 (0.86-0.93)	86.5%	81.0%	76.1%	63.7%	**.010**
Thickness GBC	0.91 (0.87-0.95)	88.5%	87.4%	82.7%	61.5%	.094

ONH = optic nerve head.

Metrics are shown as areas under the receiver operating characteristic curves (AUROC) and sensitivities at fixed specificities (Spec.) for each gradient boosting classifier (GBC). Significance was determined using a paired bootstrap test. Bolded *P*-values indicate statistically significant difference with $P \leq .05$.

AUROCs for classifying eyes as healthy or glaucomatous for all 5 evaluated GBCs and sensitivities at fixed specificities are presented in Table 2 (see Figure 1 which also includes AUROC results for cpRNFL thickness). The diagnostic accuracy of the full GBC (AUROC = 0.93; 95% CI, 0.89-0.96) was significantly better than that of both the ONH GBC (AUROC = 0.91; 95% CI, 0.86-0.94; $P = 0.036$) and the vessel density GBC (AUROC = 0.90; 95% CI, 0.86-0.93; $P = .010$). Sensitivities at each of the chosen fixed specificities were similar across GBC models (Supplemental Tables 1 and 2).

All GBCs showed significantly better diagnostic accuracy than all superficial and deep layer macula OCTA vessel density measurements (macula vessel density AUROCs ranged from 0.64 to 0.84; all comparisons, $P \leq .006$) and the full GBC showed significantly better diagnostic accuracy than all ONH cpRNFL thickness measurements (ONH cpRNFL thickness AUROCs ranged from 0.85 to 0.89; all comparisons $P \leq .014$). The full GBC did not, however, improve classification compared to 1 of 9 GCC thickness measurements (whole-image GCC thickness; $P = .099$) and 2 of 8 ONH OCTA vessel density measurements (whole-image vessel density; $P = .113$; circumpapillary vessel density; $P = .095$). AUROC comparisons among all GBCs and all investigated OCTA and OCT parameters are shown in Supplemental Table 2.

Figure 2 shows the estimated probability of glaucoma distribution for all GBCs and indicates that images from glaucoma eyes were more accurately identified than images from healthy eyes. The distribution of probabilities was most accurate for the full GBC, which estimated more healthy eyes as having between 0% and 10% probability of glaucoma and more glaucoma eyes as having between 90% and 100% probability of glaucoma than other GBCs. Figure 3 shows the mean relative influence of each investigated parameter included in the full GBC and indicates that, for the current study population, the best classifier model was a combination of macular GCC thickness and ONH circumpapillary vessel density measurements. This finding suggests that combining tissue thickness and vessel density measurements obtained from both macula and ONH images may improve the classification of early to moderate glaucoma compared to any of the investigated imaging protocols alone.

DISCUSSION

THE CURRENT STUDY COMPARED GBCS TRAINED USING combinations of whole image and regional OCTA and OCT macula and optic nerve head parameters to individual OCTA and OCT parameters for classifying images from healthy and glaucoma eyes. In the best case, the full GBC (which incorporated all OCTA and OCT parameters) showed better diagnostic accuracy than all but 3 individual parameters. GBCs performed well at the classification task with AUROCs ranging from 0.90 to 0.93. These results show promise for combining structural measurements (ie, vessel density and tissue thickness) obtained from 2 Avanti scanning protocols (ie, macula and ONH) for improved detection of early to moderate glaucoma. To the best of the current authors' knowledge, this is the first study to combine both vessel density and tissue thickness in a single classifier model. However, it is unclear whether the difference in whole AUROCs are of primary clinical importance because high sensitivities at low specificities contribute substantially to AUROC areas. Rather, sensitivities at high specificities may be more clinically relevant. Results shown in Supplemental Table 1 indicate that the full GBC was more sensitive at 90% specificity than all standard parameters investigated. Two macula GCC thickness parameters, 6 ONH vessel density parameter, and 1 cpRNFL parameter were more sensitive than the least sensitive GBC (ONH GBC).

Other studies have investigated the combination of multiple individual structural parameters for classifying eyes as healthy or glaucomatous.[43–45] Blumberg et al.[43] compared the diagnostic performance of 19 individual ONH and RNFL Cirrus OCT parameters to a multivariate predictive model using logistic regression. The multivariate model improved the discrimination between glaucomatous and nonglaucomatous eyes (AUROC = 0.892) compared to the best single RNFL parameters (average RNFL, AUROC = 0.855). However, this improvement was not statistically significant. Baskaran et al.[44] showed that, in early glaucoma (MD ≥ −6.0 dB) the diagnostic performances of linear discriminant analysis (LDA) and Classification and Regression Tree combining Cirrus OCT ONH and RNFL parameters were similar to those of any single parameter investigated. For comparisons including eyes with early to moderate glaucoma (MD ≥ −12.0 dB); however, both the Classification And Regression Tree model (AUROC = 0.99) and the LDA (AUROC = 0.94) improved diagnostic accuracy compared to that of any of the single parameters (AUROC range = 0.61-0.89). Yoshida et al.[45] used random forest classification to discriminate between glaucomatous and healthy eyes, using a total of 151 OCT (Topcon, Tokyo, Japan) peripapillary RNFL, macular RNFL, and ganglion cell-inner plexiform layer parameters. Diagnostic performance of the random forest combination of parameters (AUROC = 0.985) was significantly better than any individual parameter. Classifier performance reported in the study by Yoshida and associates[45] should be compared to performance in the current study with caution because of their inclusion of several advanced glaucoma eyes (range, MD = 1.8 to −23.2 dB) possibly driving the very large AUROCs (although the average MD was −5.6 dB, similar to that reported in the current study).

Numerous other studies have attempted to improve diagnostic accuracy in glaucoma by combining both anatomical

and functional measurements and have shown these combinations to be superior to single structures or functional measurements.[12,46,47] In particular, several studies have investigated different ML algorithms to combine structural and VF measurements to assess diagnostic accuracy in healthy and glaucomatous eyes.[46,48–51] Combining OCTA measurements with functional measurements using ML classifiers is a future research topic of the present group.

Results from the current study confirm that combining structural measurements using machine learning classifiers (and LDA) can improve classification of healthy and glaucomatous eyes. The magnitude of the improvement varies among methods based on the parameters used in the models and the characteristics of the population, particularly disease severity. However, combining structural measurements for detection of early to moderate disease, as suggested specifically by the current study, is not without limitations. For instance, clinicians may be limited to a single imaging evaluation at each visit due to time constraints or technician availability. This issue theoretically could be resolved by using a wide-angle imaging protocol with a field of view that included both the macula and the ONH regions.

This study has limitations. It may be suggested that including a large number of parameters in each GBC resulted in classifier over-fitting. However, 10-fold cross-validation was used to provide out-of-sample predictions for each logistic and GBC to avoid overly optimistic estimates of accuracy. In addition, an increased sample size would allow division of available data into independent training and test sets. These authors believe that the use of cross-validation in the current study is an acceptable substitute and, given the limited sample size, likely is a better method of assessing classifier performance. In addition, significantly more glaucoma patients than healthy participants had hypertension and diabetes (Table 1), both of which can affect blood flow. Following the recommendations of Janes and Pepe[52] for adjusted AUROC (adjusting for covariates which impact marker observations among controls), an exploratory analysis of differences was performed in vessel density measurements among healthy subjects with and without hypertension. No significant differences were found in any macula or ONH vessel density measurements (all $P > .104$) and thus did not pursue an adjusted analysis. Due to the low number of diabetic healthy subjects, the authors were unable to adjust for this covariate in any analysis.

In conclusion, the current results indicate that machine learning gradient-boosting classifiers combining OCTA and OCT macula and optic nerve head measurements can improve diagnostic accuracy in early to moderate glaucoma compared to most but not all single parameters. Such techniques could be incorporated into instrument software to improve clinical usefulness.

ALL AUTHORS HAVE COMPLETED AND SUBMITTED THE ICMJE FORM FOR DISCLOSURE OF POTENTIAL CONFLICTS OF INTEREST and none were reported.

Funding/Support: This work was supported by US National Institutes of Health/National Eye Institute (Bethesda, Maryland) grants R01 EY029058, R21 EY027945, P30 EY022589, R01 EY027510, and K12 EY024225; and by an unrestricted grant from Research to Prevent Blindness (New York, New York).

Financial Disclosures: L.M.Z. has received research support from Carl Zeiss Meditec, Heidelberg Engineering, Optovue, and Topcon Medical Systems. R.N.W. is a consultant for Aerie Pharmaceuticals, Allergan, Bausch & Lomb, Eyenovia, Implantdata, and Novartis; and has received research support from Bausch &Lomb, Carl Zeiss Meditec, Centervue, Heidelberg Engineering, Konan Medical, Optovue, and Research to Prevent Blindness. All other authors have reported that they have no relationships relevant to the contents of this paper to disclose.

REFERENCES

1. Akagi T, Iida Y, Nakanishi H, et al. Microvascular density in glaucomatous eyes with hemifield visual field defects: an optical coherence tomography angiography study. *Am J Ophthalmol* 2016;168:237–249.
2. Jia Y, Bailey ST, Hwang TS, et al. Quantitative optical coherence tomography angiography of vascular abnormalities in the living human eye. *Proc Natl Acad Sci U S A* 2015;112:E2395–E2402.
3. Jia Y, Morrison JC, Tokayer J, et al. Quantitative OCT angiography of optic nerve head blood flow. *Biomed Opt Express* 2012;3:3127–3137.
4. Moghimi S, Bowd C, Zangwill LM, et al. Measurement floors and dynamic ranges of OCT and OCT angiography in glaucoma. *Ophthalmology* 2019;126:980–988.
5. Rao HL, Pradhan ZS, Weinreb RN, et al. Relationship of optic nerve structure and function to peripapillary vessel density measurements of optical coherence tomography angiography in glaucoma. *J Glaucoma* 2017;26:548–554.
6. Rao HL, Pradhan ZS, Weinreb RN, et al. Regional comparisons of optical coherence tomography angiography vessel density in primary open-angle glaucoma. *Am J Ophthalmol* 2016;171:75–83.
7. Suh MH, Zangwill LM, Manalastas PIC, et al. Deep retinal layer microvasculature dropout detected by the optical coherence tomography angiography in glaucoma. *Ophthalmology* 2016;123:2509–2518.
8. Yarmohammadi A, Zangwill LM, Diniz A, et al. Optical coherence tomography angiography vessel density in healthy, glaucoma suspect, and glaucoma eyes. *Invest Ophthalmol Vis Sci* 2016;57:451–459.
9. Yarmohammadi A, Zangwill LM, Diniz-Filho A, et al. Relationship between optical coherence tomography angiography vessel density and severity of visual field loss in glaucoma. *Ophthalmology* 2016;123:2498–2508.

10. Wang XL, Jiang CH, Ko T, et al. Correlation between optic disc perfusion and glaucomatous severity in patients with open-angle glaucoma: an optical coherence tomography angiography study. *Graef Arch Clin Exp* 2015;253:1557–1564.
11. Moghimi S, Zangwill LM, Penteado RC, et al. Macular and optic nerve head vessel density and progressive retinal nerve fiber layer loss in glaucoma. *Ophthalmology* 2018;125:1720–1728.
12. Bizios D, Heijl A, Bengtsson B. Trained artificial neural network for glaucoma diagnosis using visual field data: a comparison with conventional algorithms. *J Glaucoma* 2007;16:20–28.
13. Bowd C, Chan K, Zangwill LM, et al. Comparing neural networks and linear discriminant functions for glaucoma detection using confocal scanning laser ophthalmoscopy of the optic disc. *Invest Ophthalmol Vis Sci* 2002;43:3444–3454.
14. Bowd C, Chan K, Zangwill LM, et al. Comparison of learning neural networks and linear discriminate functions to discriminate between glaucomatous and non-glaucomatous eyes using HRT optic disc topograhy parameters. *Invest Ophthalmol Vis Sci* 2001;42:s118.
15. Bowd C, Medeiros FA, Zhang Z, et al. Relevance vector machine and support vector machine classifier analysis of scanning laser polarimetry retinal nerve fiber layer measurements. *Invest Ophthalmol Vis Sci* 2005;46:1322–1329.
16. Brigatti L, Hoffman D, Caprioli J. Neural networks to identify glaucoma with structural and functional measurements. *Am J Ophthalmol* 1996;121:511–521.
17. Burgansky-Eliash Z, Wollstein G, Chu T, et al. Optical coherence tomography machine learning classifiers for glaucoma detection: a preliminary study. *Invest Ophthalmol Vis Sci* 2005;46:4147–4152.
18. Chan K, Lee TW, Sample PA, Goldbaum MH, Weinreb RN, Sejnowski TJ. Comparison of machine learning and traditional classifiers in glaucoma diagnosis. *IEEE Trans Biomed Eng* 2002;49:963–974.
19. Christopher M, Belghith A, Bowd C, et al. Performance of deep learning architectures and transfer learning for detecting glaucomatous optic neuropathy in fundus photographs. *Sci Rep* 2018;8:16685.
20. Christopher M, Belghith A, Weinreb RN, et al. Retinal nerve fiber layer features identified by unsupervised machine learning on optical coherence tomography scans predict glaucoma progression. *Invest Ophthalmol Vis Sci* 2018;59:2748–2756.
21. Goldbaum MH, Sample PA, Chan K, et al. Comparing machine learning classifiers for diagnosing glaucoma from standard automated perimetry. *Invest Ophthalmol Vis Sci* 2002;43:162–169.
22. Goldbaum MH, Sample PA, White H, et al. Interpretation of automated perimetry for glaucoma by neural network. *Invest Ophthalmol Vis Sci* 1994;35:3362–3373.
23. Hothorn T, Lausen B. Bagging tree classifiers for laser scanning images: a data- and simulation-based strategy. *Artif Intell Med* 2003;27:65–79.
24. Li A, Cheng J, Wong DWK, Liu J. Integrating holistic and local deep features for glaucoma classification. *Conf Proc IEEE Eng Med Biol Soc* 2016;2016:1328–1331.
25. Lietman T, Eng J, Katz J, Quigley HA. Neural networks for visual field analysis: how do they compare with other algorithms? *J Glaucoma* 1999;8:77–80.
26. Liu S, Graham S, Shulz A, et al. A deep learning-based algorithm identifies glaucomatous discs using monoscopic fundus photographs. *Opthalmol Glaucoma* 2018;1:15–22.
27. Madsen EM, Yolton RL. Demonstration of a neural network expert system for recognition of glaucomatous visual field changes. *Mil Med* 1994;159:553–557.
28. Mardin CY, Hothorn T, Peters A, Junemann AG, Nguyen NX, Lausen B. New glaucoma classification method based on standard Heidelberg Retina Tomograph parameters by bagging classification trees. *J Glaucoma* 2003;12:340–346.
29. Medeiros FA, Jammal AA, Thompson AC. From machine to machine: an OCT-trained deep learning algorithm for objective quantification of glaucomatous damage in fundus photographs. *Ophthalmology* 2019;126:513–521.
30. Mutlukan E, Keating D. Visual field interpretation with a personal computer based neural network (Pt. 3). *Eye* 1994;8:321–323.
31. Phan S, Satoh S, Yoda Y, et al. Evaluation of deep convolutional neural networks for glaucoma detection. *Jpn J Ophthalmol* 2019;63:276–283.
32. Swindale NV, Stjepanovic G, Chin A, Mikelberg FS. Automated analysis of normal and glaucomatous optic nerve head topography images. *Invest Ophthalmol Vis Sci* 2000;41:1730–1742.
33. Wroblewski D, Francis BA, Chopra V, et al. Glaucoma detection and evaluation through pattern recognition in standard automated perimetry data. *Graefes Arch Clin Exp Ophthalmol* 2009;247:1517–1530.
34. Zangwill LM, Chan K, Bowd C, et al. Heidelberg retina tomograph measurements of the optic disc and parapapillary retina for detecting glaucoma analyzed by machine learning classifiers. *Invest Ophthalmol Vis Sci* 2004;45:3144–3151.
35. Sample PA, Girkin CA, Zangwill LM, et al. The African Descent and Glaucoma Evaluation Study (ADAGES): design and baseline data. *Arch Ophthalmol* 2009;127:1136–1145.
36. Liu L, Jia Y, Takusagawa HL, et al. Optical coherence tomography angiography of the peripapillary retina in glaucoma. *JAMA Ophthalmol* 2015;133:1045–1052.
37. Schapire RE, Freund Y, Bartlett P, Lee WS. Boosting the margin: a new explanation for the effectiveness of voting methods. *Ann Stat* 1998;26:1651–1686.
38. Caruana R, Niculescu-Mizil A. An empirical comparison of supervised learning algorithms. Presented at Proc.Int. Conf. Machine Learn., 23rd, Pittsburgh, PA
39. Friedman JH. Greedy function approximation: a gradient boosting machine. *Ann Stat* 2001;29:1189–1232.
40. Bender R, Lange S. Adjusting for multiple testing–when and how? *J Clin Epidemiol* 2001;54:343–349.
41. Ridgeway G. Generalized Boosted Models: A Guide to the gbm Package. R Software; Vienna, Austria. Available at: ; 2019. https://cran.r-project.org/web/packages/gbm/vignettes/gbm.pdf;. Accessed April 22, 2020.
42. Greenwell B, Boehmke B, Cunningham J. gbm: Generalized Boosted Regression Models. R version 2.1.5 Software; Vienna, Austria. Available at: https://cran.r-project.org/web/packages/gbm/gbm.pdf. Accessed April 22, 2020.
43. Blumberg DM, Dale E, Pensec N, et al. Discrimination of glaucoma patients from healthy individuals using combined parameters from spectral-domain optical coherence tomography in an African American population. *J Glaucoma* 2016;25:E196–E203.

44. Baskaran M, Ong EL, Li JL, et al. Classification algorithms enhance the discrimination of glaucoma from normal eyes using high-definition optical coherence tomography. *Invest Ophthalmol Vis Sci* 2012;53:2314–2320.
45. Yoshida T, Iwase A, Hirasawa H, et al. Discriminating between glaucoma and normal eyes using optical coherence tomography and the "random forests" classifier. *PLoS One* 2014;9:e106117.
46. Bowd C, Hao J, Tavares IM, et al. Bayesian machine learning classifiers for combining structural and functional measurements to classify healthy and glaucomatous eyes. *Invest Ophthalmol Vis Sci* 2008;49:945–953.
47. Boland MV, Quigley HA. Evaluation of a combined index of optic nerve structure and function for glaucoma diagnosis. *BMC Ophthalmol* 2011;11:6.
48. Racette L, Chiou CY, Hao J, et al. Combining functional and structural tests improves the diagnostic accuracy of relevance vector machine classifiers. *J Glaucoma* 2010;19:167–175.
49. Kim SJ, Cho KJ, Oh S. Development of machine learning models for diagnosis of glaucoma. *PLoS One* 2017;12:e0177726.
50. Raza AS, Zhang X, De Moraes CGV, et al. Improving glaucoma detection using spatially correspondent clusters of damage and by combining standard automated perimetry and optical coherence tomography. *Invest Ophthalmol Vis Sci* 2014;55:612–624.
51. Shigueoka LS, Vasconcellos JPC, Schimiti RB, et al. Automated algorithms combining structure and function outperform general ophthalmologists in diagnosing glaucoma. *PLoS One* 2018;13:e0207784.
52. Janes H, Pepe MS. Adjusting for covariate effects on classification accuracy using the covariate-adjusted receiver operating characteristic curve. *Biometrika* 2009;96(2):371–382.